

# Test of the hadronic interaction model EPOS with air shower data

W.D. Apel<sup>1</sup>, J.C. Arteaga<sup>1‡</sup>, F. Badea<sup>1</sup>, K. Bekk<sup>1</sup>,  
 M. Bertaina<sup>2</sup>, J. Blümer<sup>1,3</sup>, H. Bozdog<sup>1</sup>, I.M. Brancus<sup>4</sup>,  
 M. Brüggemann<sup>5</sup>, P. Buchholz<sup>5</sup>, E. Cantoni<sup>3,7</sup>, A. Chiavassa<sup>2</sup>,  
 F. Cossavella<sup>3</sup>, K. Daumiller<sup>1</sup>, V. de Souza<sup>3§</sup>, F. Di Pierro<sup>2</sup>,  
 P. Doll<sup>1</sup>, R. Engel<sup>1</sup>, J. Engler<sup>1</sup>, M. Finger<sup>1</sup>, D. Fuhrmann<sup>6</sup>,  
 P.L. Ghia<sup>7</sup>, H.J. Gils<sup>1</sup>, R. Glasstetter<sup>6</sup>, C. Grupen<sup>5</sup>,  
 A. Haungs<sup>1</sup>, D. Heck<sup>1</sup>, J.R. Hörandel<sup>3||</sup>, T. Huege<sup>1</sup>, P.G. Isar<sup>1</sup>,  
 K.-H. Kampert<sup>6</sup>, D. Kang<sup>3</sup>, D. Kickelbick<sup>5</sup>, H.O. Klages<sup>1</sup>,  
 Y. Kolotaev<sup>5</sup>, P. Luczak<sup>8</sup>, H.J. Mathes<sup>1</sup>, H.J. Mayer<sup>1</sup>,  
 J. Milke<sup>1</sup>, B. Mitrica<sup>4</sup>, C. Morello<sup>7</sup>, G. Navarra<sup>2</sup>, S. Nehls<sup>1</sup>,  
 J. Oehlschläger<sup>1</sup>, S. Ostapchenko<sup>1¶</sup>, S. Over<sup>5</sup>, M. Petcu<sup>4</sup>,  
 T. Pierog<sup>1</sup>, H. Rebel<sup>1</sup>, M. Roth<sup>1</sup>, H. Schieler<sup>1</sup>, F. Schröder<sup>1</sup>,  
 O. Sima<sup>9</sup>, M. Stümpert<sup>3</sup>, G. Toma<sup>4</sup>, G.C. Trinchero<sup>7</sup>,  
 H. Ulrich<sup>1</sup>, J. van Buren<sup>1</sup>, W. Walkowiak<sup>5</sup>, A. Weindl<sup>1</sup>,  
 J. Wochele<sup>1</sup>, M. Wommer<sup>1</sup>, J. Zabierowski<sup>8</sup>

<sup>1</sup> Institut für Kernphysik, Forschungszentrum Karlsruhe, 76021 Karlsruhe, Germany

<sup>2</sup> Dipartimento di Fisica Generale dell'Università, 10125 Torino, Italy

<sup>3</sup> Institut für Experimentelle Kernphysik, Universität Karlsruhe, 76021 Karlsruhe, Germany,

<sup>4</sup> National Institute of Physics and Nuclear Engineering, 7690 Bucharest, Romania

<sup>5</sup> Fachbereich Physik, Universität Siegen, 57068 Siegen, Germany

<sup>6</sup> Fachbereich Physik, Universität Wuppertal, 42097 Wuppertal, Germany

<sup>7</sup> Istituto di Fisica dello Spazio Interplanetario, INAF, 10133 Torino, Italy

<sup>8</sup> Soltan Institute for Nuclear Studies, 90950 Lodz, Poland

<sup>9</sup> Department of Physics, University of Bucharest, 76900 Bucharest, Romania

**Abstract.** Predictions of the hadronic interaction model EPOS 1.61 as implemented in the air shower simulation program CORSIKA are compared to observations with the KASCADE experiment. The investigations reveal that the predictions of EPOS are not compatible with KASCADE measurements. The discrepancies seen are most likely due to use of a set of inelastic hadronic cross sections that are too high.

‡ now at Institute of Physics and Mathematics, Universidad Michoacana, Morelia, Mexico

§ now at Universidade de São Paulo, Instituto de Física de São Carlos, Brasil

|| corresponding author email:j.horandel@astro.ru.nl, now at Department of Astrophysics, Radboud University Nijmegen, The Netherlands

¶ now at Norwegian University, Trondheim, Norway

PACS numbers: 13.85.-t, 13.85.Tp, 96.50.S-, 96.50.sb, 96.50.sd

*Keywords:* air showers, high-energy interactions, cosmic rays

Submitted to: *J. Phys. G: Nucl. Phys.*

## 1. Introduction

When high-energy cosmic rays penetrate the Earth's atmosphere they initiate cascades of secondary particles — the extensive air showers. Objective of air shower detectors is to derive information about the shower inducing primary particle from the registered secondary particles. Addressing astrophysical questions with air-shower data necessitates the understanding of high-energy interactions in the atmosphere. Or, in reversion, the interpretation of properties of primary radiation derived from air-shower measurements depends on the understanding of the complex processes during the development of air showers. In the last decade significant progress has been achieved in the interpretation of air shower data and main properties of the primary cosmic radiation have been measured. At energies around  $10^6$  GeV the mass composition of cosmic rays has been investigated and energy spectra for groups of elements could be derived [1, 2]. It could be shown that the knee in the all-particle energy spectrum at about  $4 \cdot 10^6$  GeV is caused by a cut-off in the energy spectra of the light elements (protons and helium). Despite of this progress, detailed investigations indicate inconsistencies in the interpretation of air shower data [1, 3, 4, 5, 6, 7, 8]. Thus, one of the goals of KASCADE (Karlsruhe Shower Core and Array DEtector) is to investigate high-energy interactions in the atmosphere and to improve contemporary models to describe such processes.

For air shower interpretation the understanding of multi-particle production in hadronic interactions with a small momentum transfer is essential [9]. Due to the energy dependence of the coupling constant  $\alpha_s$ , soft interactions cannot be calculated within QCD using perturbation theory. Instead, phenomenological approaches have been introduced in different models. These models are the main source of uncertainties in simulation codes to calculate the development of extensive air showers, such as the program CORSIKA [10]. Several codes to describe hadronic interactions at low energies ( $E < 200$  GeV; e.g. GHEISHA [11] and FLUKA [12, 13]) as well as high energies (e.g. DPMJET [14], QGSJET [15, 16, 17], SIBYLL [18], and EPOS [19, 20]) have been embedded in CORSIKA.

The test of interaction models necessitates detailed measurements of several shower components. The KASCADE experiment [21] with its multi-detector set-up, registering simultaneously the electromagnetic, muonic, and hadronic shower components is particularly suited for such investigations. The information derived on properties of high-energy interactions from air shower observations is complementary

to measurements at accelerator experiments since different kinematical and energetic regions are probed.

In previous investigations [7, 8] the models QGSJET versions 98 and 01 [15], VENUS [22], SIBYLL versions 1.6 [23] and 2.1 [18], DPMJET [14], and NEXUS [24] have been studied. The analyses presented in this article focus on the interaction model EPOS, version 1.61. This model is a recent development, historically emerging from the VENUS and NEXUS codes.

EPOS is a consistent quantum mechanical multiple scattering approach based on partons and strings, where cross sections and the particle production are calculated consistently, taking into account energy conservation in both cases (unlike other models where energy conservation is not considered for cross section calculations [25]). A special feature is the explicit treatment of projectile and target remnants, leading to a better description of baryon and antibaryon production than in other models used for cosmic-ray analysis. Motivated by the data obtained by the RHIC experiments, nuclear effects related to Cronin transverse momentum broadening, parton saturation, and screening have been introduced into EPOS. Furthermore, unlike other models, high density effects leading to collective behavior in heavy ion collisions (or lighter systems) are also taken into account. Since this model is applied to accelerator physics, many data are considered which are not a priori linked to cosmic rays and air showers. That is may be the largest difference to all other hadronic models used to simulate air showers.

## 2. Experimental set-up

### 2.1. The apparatus

The experiment KASCADE, located on site of the Forschungszentrum Karlsruhe, 110 m a.s.l., consists of several detector systems. A description of the performance of the experiment can be found elsewhere [21]. A  $200 \times 200 \text{ m}^2$  array of 252 detector stations, equipped with scintillation counters, measures the electromagnetic and, below a lead/iron shielding, the muonic parts of air showers. In its center, an iron sampling calorimeter of  $16 \times 20 \text{ m}^2$  area detects hadronic particles. The calorimeter is equipped with 11 000 warm-liquid ionization chambers arranged in nine layers. Due to its fine segmentation ( $25 \times 25 \text{ cm}^2$ ), energy, position, and angle of incidence can be measured for individual hadrons. A detailed description of the calorimeter and its performance can be found in [26], it has been calibrated with a test beam at the SPS at CERN up to 350 GeV particle energy [27].

### 2.2. Observables and event selection

The position of the shower axis and the angle of incidence of a cascade are reconstructed by the array detectors. The total numbers of electrons  $N_e$  and muons  $N_\mu$  are determined by integrating their lateral distributions. In case of muons, the truncated muon number  $N_\mu^{tr}$  is used for experimental reasons. It is the number of muons integrated in the distance

range 40 – 200 m from the shower axis. For a detailed description of the reconstruction algorithms see [28]. The position of the shower axis is reconstructed with an accuracy better than 2 m and the angle of incidence better than  $0.5^\circ$ .

The hadrons in the calorimeter are reconstructed by a pattern recognition algorithm, optimized to recognize as many hadrons in a shower core as possible. Details can be found in [28]. Hadrons of equal energy can still be separated with a probability of 50% at a distance of 40 cm. The reconstruction efficiency rises from 70% at 50 GeV to nearly 100% at 100 GeV. The energy resolution improves from 30% at 50 GeV to 15% at  $10^4$  GeV. The hadron number  $N_h$  and hadronic energy sum  $\sum E_h$  are determined by the sum over all hadrons in a distance up to 10 m from the shower axis. A correction for the missing area beyond the boundaries of the calorimeter is applied. In the following,  $N_h$  and  $\sum E_h$  are given for a threshold of 100 GeV, but also hadronic shower sizes for higher thresholds up to 500 GeV have been investigated. The observable  $\sum E_h$  includes also energy of hadrons which could not be reconstructed independently, because they are too close to each other. It shows up in the simulated and experimental data in the same manner.

To be accepted for the analysis, an air shower has to fulfill several requirements: at least one hadron has been reconstructed in the calorimeter with an energy larger than 50 GeV, the shower axis is located inside the calorimeter, the electromagnetic shower size  $N_e$  is larger than  $10^4$ , the truncated muon number  $N_\mu^{tr}$  is larger than  $10^3$ , i.e. the primary energy is greater than about  $3 \cdot 10^5$  GeV, and the reconstructed zenith angle is smaller than  $30^\circ$ . For Figs. 2 and 6 different selection criteria have been applied [1]. Namely: the reconstructed shower axis has to be within 91 m from the center of the array, the age parameter  $s$ , obtained through a fit of a NKG function to the lateral distribution of the electromagnetic component has to be in the interval  $0.2 < s < 2.1$ , and only showers with  $\lg N_e \geq 4.8$ ,  $\lg N_\mu^{tr} \geq 3.6$ , as well as a zenith angle  $< 18^\circ$  are considered.

### 2.3. Simulations

The shower simulations were performed using CORSIKA. Hadronic interactions at low energies were modeled using the FLUKA code [12, 13]. High-energy interactions were treated with EPOS 1.61 [19, 20] ( $E > 80$  GeV) as well as QGSJET 01 [15] ( $E > 200$  GeV). The latter has been chosen for reference in order to compare the results discussed in the present article to previous publications [7, 8]. Showers initiated by primary protons and iron nuclei have been simulated. The simulations covered the energy range  $10^5 - 10^8$  GeV with zenith angles in the interval  $0^\circ - 32^\circ$ . The spectral index in the simulations was  $-2.0$ . For the analysis it is converted to a slope of  $-2.7$  below and  $-3.1$  above the knee with a rigidity dependent knee position ( $3 \cdot 10^6$  GeV for protons).<sup>+</sup> The positions of the shower axes are distributed uniformly over an area exceeding the calorimeter surface by 2 m on each side. In order to determine the

<sup>+</sup> Again, Figs. 2 and 6 have been treated differently, see Ref. [1].

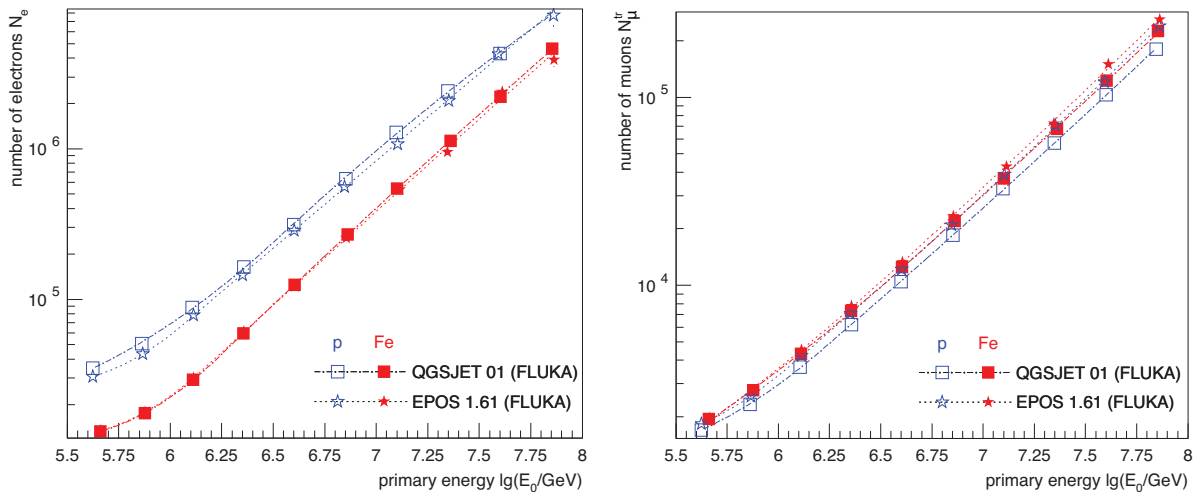


**Figure 1.** Number of electrons (*left*) and number of muons (*right*) as function of shower energy for proton and iron induced showers as predicted by the hadronic interaction models EPOS and QGSJET 01.

signals in the individual detectors, all secondary particles at ground level are passed through a detector simulation program using the GEANT package [29]. In this way, the instrumental response is taken into account and the simulated events are analyzed by the same code as the experimental data, an important aspect to avoid biases by pattern recognition and reconstruction algorithms.

The average primary energy belonging to a simulated and reconstructed number of electrons and muons is given in Fig. 1. The left panel demonstrates the  $N_e$  dependence on the primary mass. The lines through the points are drawn to guide the eye and represent five parameter fits. As in all figures errors of the mean values are plotted. But, in most cases, the error bars are smaller than the marker size. It is seen from Fig. 1 that both models yield a nearly linear dependence. Only near threshold  $N_e$  rises slowly for light primaries, namely protons. The number of muons is expected to be a good estimator for the primary energy, since, irrespective of the individual shower development, the most abundant secondaries of the interactions are pions, for which the charged species decay to muons and arrive to a large extent at the Earth's surface. This behavior is illustrated in Fig. 1 (*right*). The difference in energy for protons and iron nuclei for a fixed number of muons amounts to about 25% only for both models.

### 3. Results

#### 3.1. Primary energy correlations

The number of electrons and muons registered at ground level as function of energy for the interaction models EPOS 1.61 and QGSJET 01 is depicted in Fig. 1. For protons differences between the predictions of the two models can be recognized. These differences are less pronounced for iron induced showers. The number of electrons is

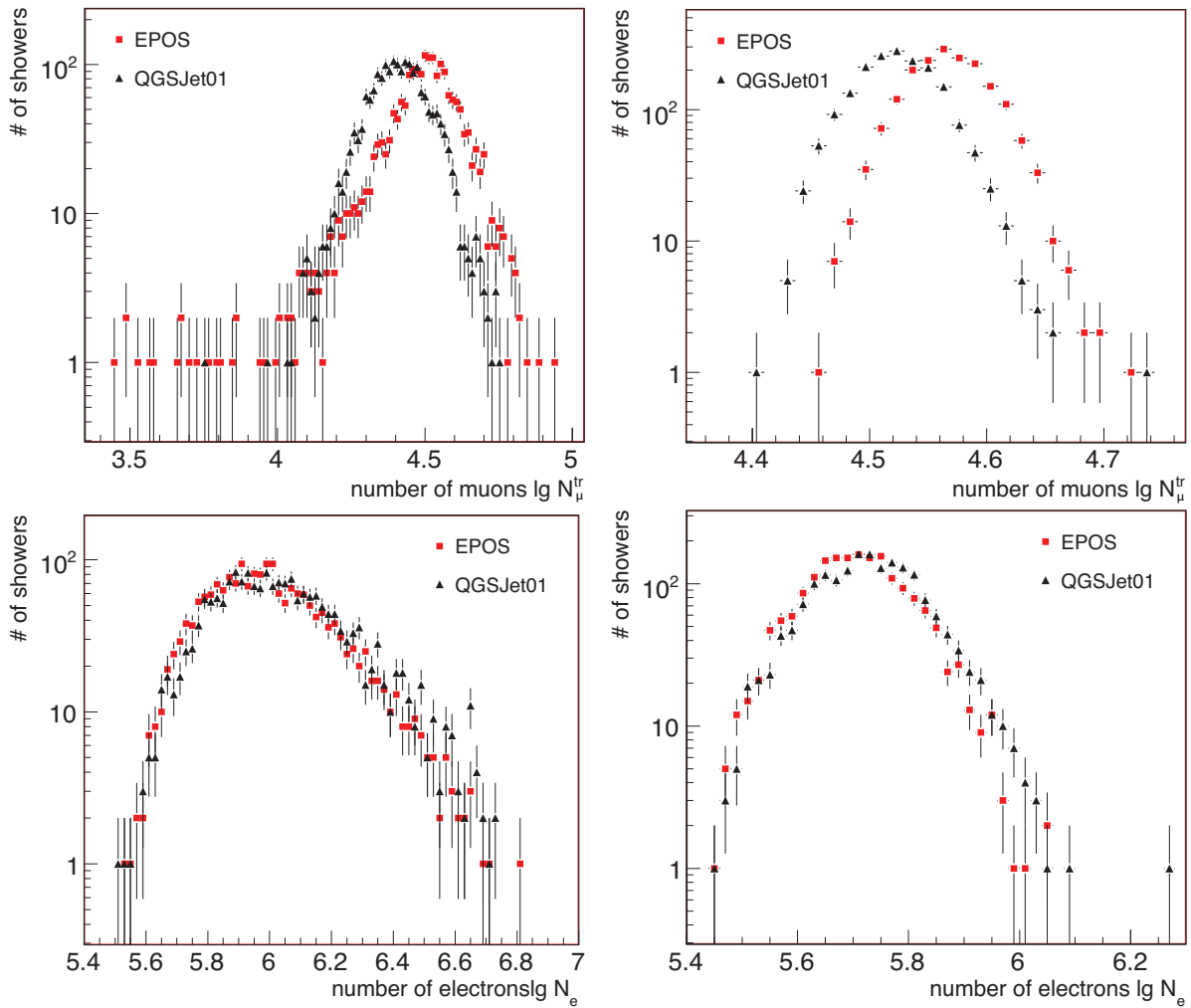


**Figure 2.** Predictions of two interaction models for the number of registered muons (*top*) and electrons (*bottom*) at ground for primary protons (*left*) and iron nuclei (*right*) with an energy of  $10^7$  GeV.

slightly lower for a fixed energy for the model EPOS and the number of muons is larger for this model as compared to QGSJET.

While mean values are shown in Fig.1, the underlying distributions are given in Fig.2. The figure displays the number of muons (*top*) and electrons (*bottom*) expected for showers with an energy of  $10^7$  GeV for primary protons (*left*) and iron nuclei (*right*). Results for EPOS are compared to predictions of the model QGSJET 01. For both primary particle species EPOS yields clearly more muons at observation level as compared to QGSJET, while the shapes of the distributions are very similar. The corresponding distributions for the number of electrons observed at ground level are very similar for both models. They agree well in shape for both, primary protons and iron nuclei. But the positions of the maxima are slightly shifted.

The relation of observed hadronic observables as function of shower energy are presented in Figs.3 and 4. They show the number of hadrons  $N_h$ , the hadronic energy

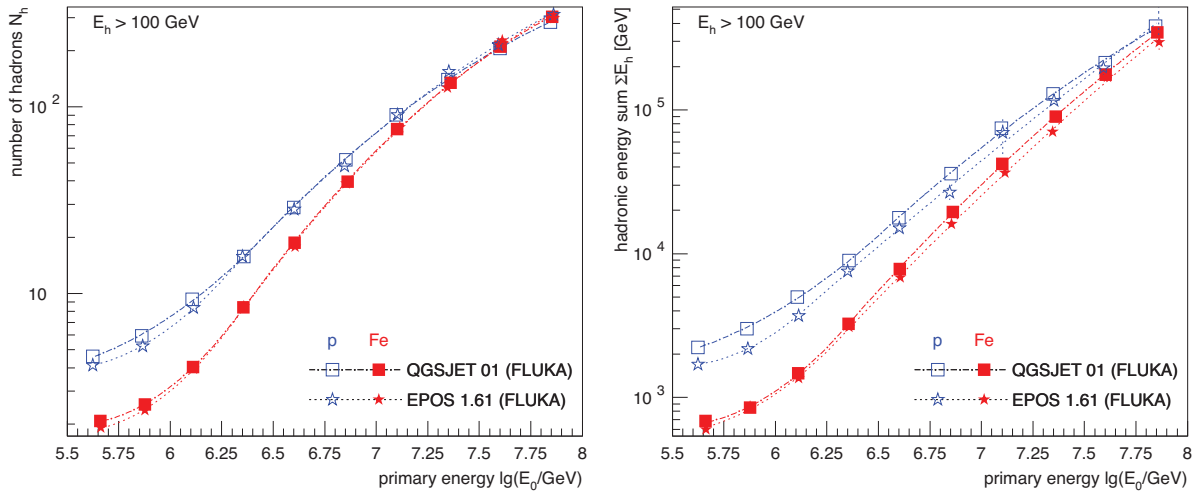


**Figure 3.** Number of hadrons (*left*) and hadronic energy sum (*right*) as function of shower energy for two interaction models and two primary particle species.

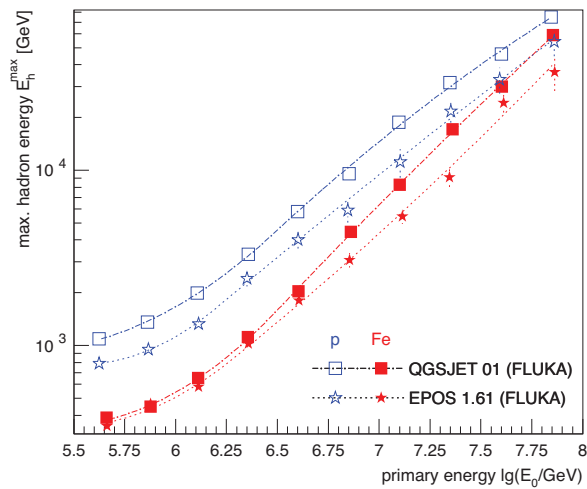


**Figure 4.** Energy of the most energetic hadron in a shower as function of shower energy for two interaction models and two primary particle species.

sum  $\sum E_h$ , and the energy of the highest energy hadron observed at ground  $E_h^{max}$ , respectively. The number of hadrons for a given energy predicted by both, EPOS and QGSJET 01 are very similar. But there is a significant difference in the hadronic energy transported to observation level. EPOS yields about 25% smaller values for  $\sum E_h$  as compared to QGSJET 01 at the same shower energy. The effect has a similar magnitude for both primary species. An even bigger difference is observed for the value of the highest-energy hadron registered at ground level. The maximum energies are reduced by up to 50% to 60% for EPOS compared to QGSJET at the same shower energy. Again, the effect is similarly strong for both primary species.

### 3.2. Electron – muon correlations

Turning our attention towards observable quantities, among the most interesting ones is the effect of the different models on the number of electrons and muons at ground level. They are used to reconstruct energy and mass of the shower inducing particles,

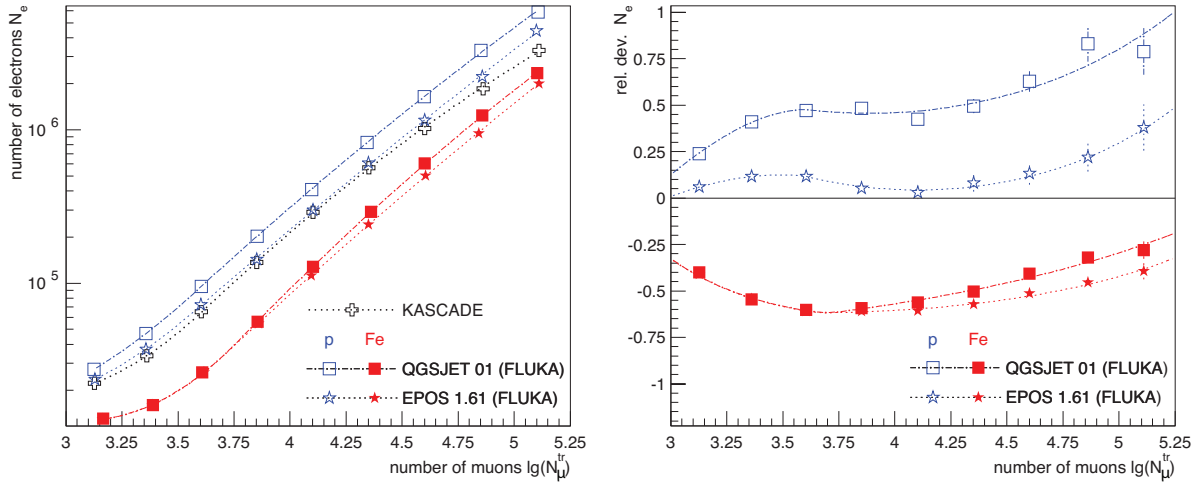


**Figure 5.** Number of electrons as function of muons for model predictions compared to KASCADE measurements. Absolute values (*left*) and relative values  $(N_e^{sim} - N_e^{meas})/N_e^{meas}$  (*right*). Predictions for two interaction models and two primary particle species are shown.

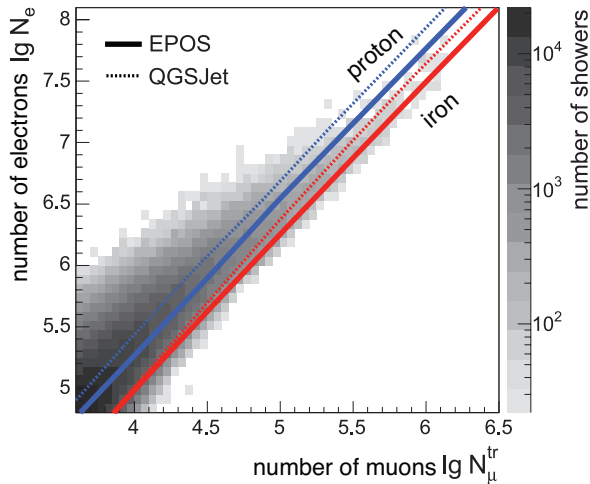


**Figure 6.** Number of electrons as function of muons ( $N_e - N_\mu$  plane). The measured two dimensional shower size distribution (grey shaded area) is compared to most probable values as predicted by two interaction models for two primary species.

e.g. by applying an unfolding algorithm [1, 30].

The average number of electrons as function of the number of muons is displayed in Fig.5 (*left*) for the two models. Predictions for primary protons and iron nuclei are compared to measured values. To emphasize the differences between the model predictions, the same data are plotted on the right hand panel in a different manner. The model predictions are shown relative to the measured values, i.e. the quantity  $(N_e^{sim} - N_e^{meas})/N_e^{meas}$  is presented. For a given muon number EPOS clearly yield less electrons ( $\approx 40\%$ ) for proton induced cascades and significantly lesser electrons for iron showers at high energies, i.e. large muon numbers. This can be understood taking Fig. 1 into account. The differences seen there for given primary energies translate into the significant discrepancies between the two models seen in the electron-muon correlation (Fig. 5).

To estimate the effects on the unfolding procedure it is useful to have a look at

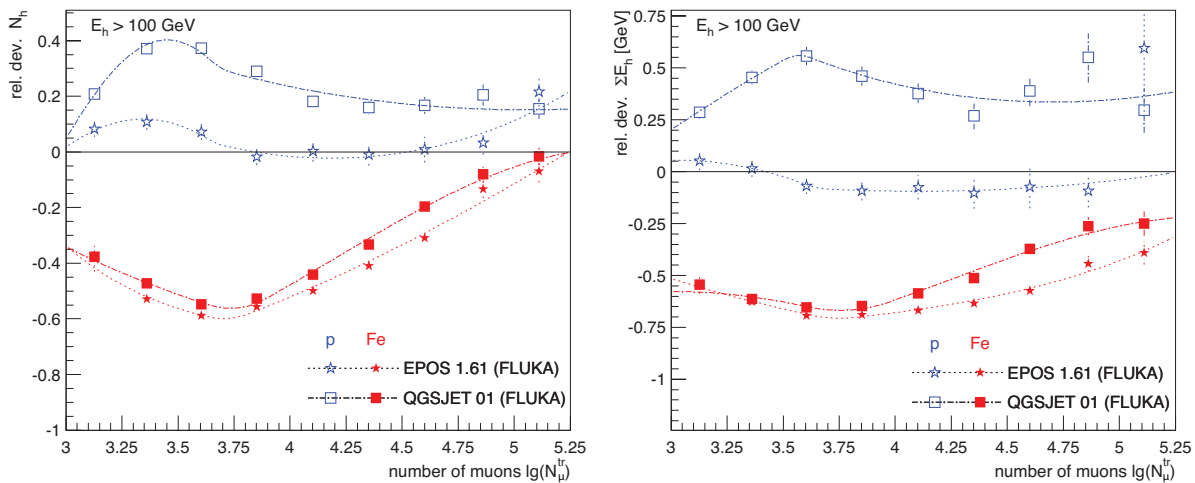


**Figure 7.** Number of hadrons observed (*left*) and reconstructed hadronic energy sum (*right*) as function of the registered number of muons for proton and iron induced showers. The predictions of two interaction models are shown relative to the measured values.

the  $N_e - N_\mu$  plane, see Fig. 6. The figure represents the measured two dimensional shower size spectrum (grey coded area). The lines correspond to most probable values for primary protons and iron nuclei as predicted by the interaction models EPOS and QGSJET. It can clearly be recognized that the lines for EPOS are shifted towards the lower right corner of the figure with respect to QGSJET. This implies, if EPOS predictions are used to derive the mass of the primary particles from the observed data a dominantly light mass composition is obtained.

To check this effect, the energy spectra for five groups of elements (as in [1]) have been unfolded from the measurements, based on EPOS predictions. In this exercise in the energy range between  $10^6$  and  $10^7$  GeV a very high flux of protons is obtained and the flux of heavy particles (iron group) is strongly suppressed. If one extrapolates direct measurements to high energies, such a behavior seems to be extremely unrealistic. This study illustrates that it would be very useful to measure the energy spectra of individual elements directly up to the knee region. Such data would be very helpful to verify the interaction codes utilized in air shower simulations.

### 3.3. Hadron – muon correlations

The differences already seen in Fig. 3 are not directly accessible in measurements, since the energy of the primary particle can not be inferred directly. To check the validity of interaction models it is therefore suitable to plot observable quantities against each other such as e.g. the number of registered hadrons or the observed hadronic energy at ground level as function of the number of muons as depicted in Fig. 7. Again, the model predictions are plotted relative to the values measured by KASCADE, i.e. the quantity  $(x_{sim} - x_{meas})/x_{meas}$  is presented.  $x$  represents  $N_h$  or  $\sum E_h$  for two interaction models and two primary particle species. In particular for primary protons for a given

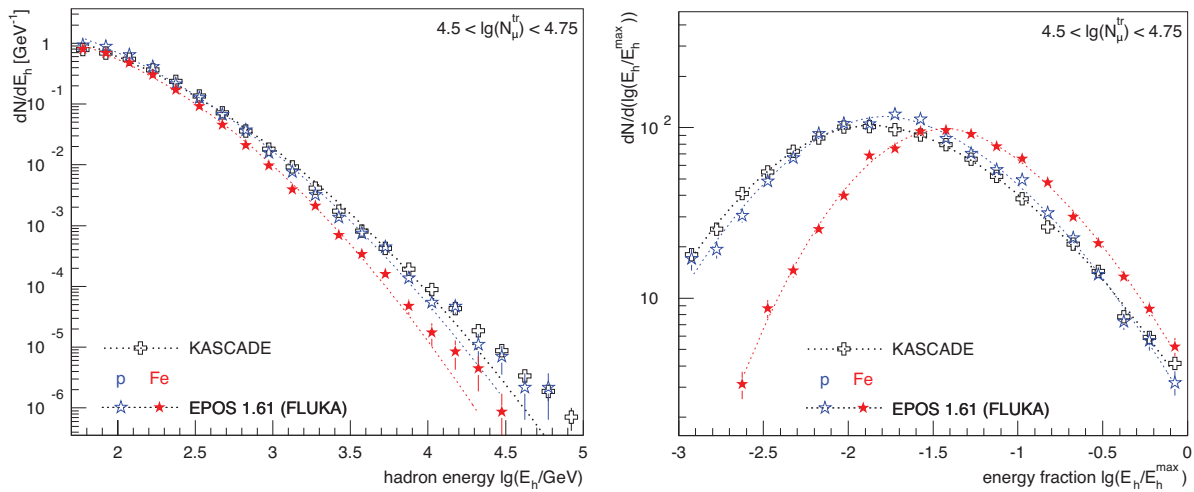


**Figure 8.** Energy spectrum of reconstructed hadrons (*left*) and fraction of the reconstructed hadron energy to the maximum hadron energy (*right*) for a given muon number interval. EPOS predictions for proton and iron induced cascades are compared to measured values.

muon number EPOS yields significantly less hadrons and delivers less hadronic energy to the observation level. It is generally assumed that in the energy range of interest the average mass composition of cosmic rays is between protons and iron. Thus, in Fig. 7 (as in Fig. 5, right) the zero line should be “bracketed” by the predictions for proton and iron induced showers, as it is the case for the model QGSJET. On the other hand, it can be recognized that for EPOS at high muon numbers (corresponding to energies around  $10^7$  GeV) the hadronic energy sums of both, proton and iron induced showers are smaller than the experimental data. The systematic uncertainty of the hadronic energy sum amounts to about 15%. Within this uncertainty the data are compatible with the EPOS predictions, assuming that all cosmic rays are protons only. However, at energies around  $10^6$  to  $10^7$  GeV this is not realistic. This implies that the EPOS predictions are not compatible with the data.

The behavior observed for the maximum hadron energy  $E_h^{max}$  registered at observation level is very similar to the situation depicted in Fig. 7 (*right*) for the hadronic energy sum. At high muon numbers EPOS yields values for  $E_h^{max}$  which are clearly below the measurements for both primary species (protons and iron nuclei) — an unrealistic scenario.

Another way to shed light on the interaction models is to investigate the energy spectra of hadrons for a given muon number interval, i.e. an approximately fixed primary energy. Hadron energy spectra as predicted by EPOS are compared to measured values in Fig. 8 (*left*). \* The muon number interval corresponds to primary energies around  $2 \cdot 10^7$  GeV. At high hadron energies EPOS underestimates the observed flux. The predictions for both primary species are below the measured values. This observation is

\* Corresponding distributions for the interaction model QGSJET have been published previously [7]. The predictions are compatible with the measured data.

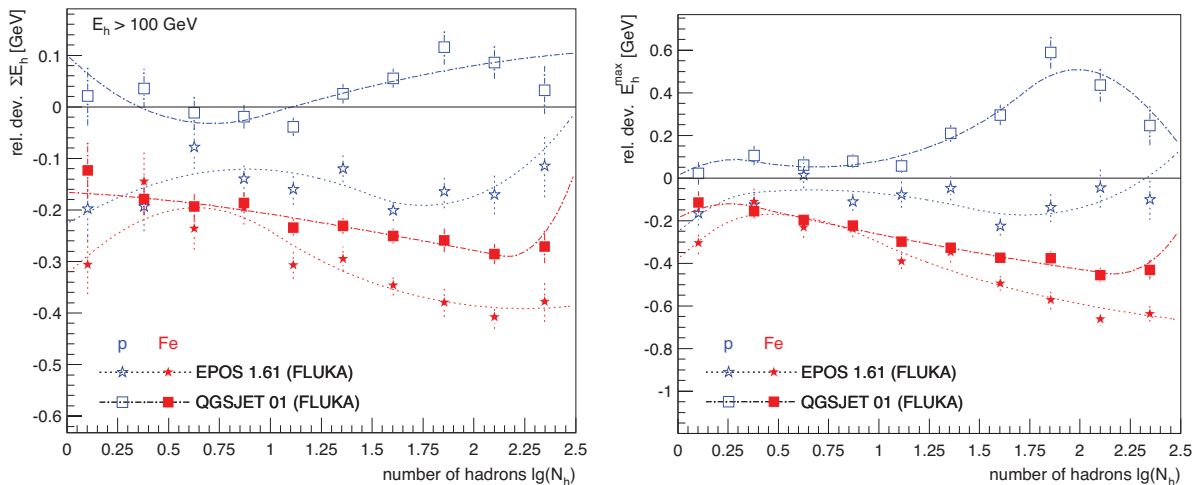


**Figure 9.** Relative hadronic energy sum ( $\sum E_h^{\text{sim}} - \sum E_h^{\text{meas}} / \sum E_h^{\text{meas}}$ ) (left) and relative maximum hadron energy (right) as function of the reconstructed number of hadrons for two interaction models and two primary particle species.

compatible with the above findings (Figs. 3 and 4), namely the relatively low hadronic energy sum and the relatively small maximum hadron energy.

Distributions of the ratio of the energy of each reconstructed hadron to the maximum hadron energy in each shower  $E_h/E_h^{\text{max}}$  are plotted in Fig. 8 (right) for the same muon interval as above. Again, EPOS predictions for two particle species are compared to measured data. As for the other observables discussed, the measurements should be “bracketed” by the predictions for proton and iron induced showers. However, the EPOS predictions exhibit a clearly different behavior. For most  $E_h/E_h^{\text{max}}$  ratios the measured values are outside the proton-iron range given by the model.

The investigations of the energy spectra confirm the above findings, that EPOS predictions are not compatible with KASCADE data.

### 3.4. Hadron – hadron correlations

In the previous discussions it has been seen already that EPOS delivers less energy in form of hadrons to ground level as compared to QGSJET 01. Therefore, it is an interesting exercise to investigate also the correlations of the purely hadronic observables with each other. Examples of such correlations are presented in Fig. 9, depicting the hadronic energy sum (left) and the maximum hadron energy per shower (right). The predicted values are again plotted relative to the measured quantities to visually magnify the differences between the model predictions. In the figure the quantities are plotted as function of the number of hadrons  $N_h$ . Due to the steeply falling energy spectrum and the  $N_h - E_0$  correlation (see Fig. 3) a sampling of the data in  $N_h$  intervals yields an enrichment of light particles. Therefore, the data are expected to look very “proton like”. Indeed, for QGSJET the proton predictions are very close to the “zero line”, i.e. to the KASCADE measurements. It should also be mentioned that (within the

error bars) the QGSJET predictions “bracket” the measured values. In contrast, the EPOS predictions for both primary species are below zero for both observables shown in the figure. The EPOS predictions for protons are at the lower bound of the 15% systematic uncertainty for the hadronic energy sum. Thus, they are barely compatible with the data. However, it should be stressed that the QGSJET predictions for protons really are at values around zero as expected. This indicates that the systematic effects might be smaller than estimated and the EPOS predictions are not compatible with the measurements. From all observables investigated the hadron-hadron correlations exhibit the strongest incompatibility between the EPOS predictions and the KASCADE data.

#### 4. Summary and conclusions

Predictions of air shower simulations using the CORSIKA code with the hadronic interaction models EPOS 1.61 and QGSJET 01 have been compared to measurements of the KASCADE experiment. Various observables of the electromagnetic, muonic, and hadronic component have been investigated and the correlations between them have been analyzed. They have been used to check the compatibility of the EPOS predictions with the KASCADE measurements.

The findings can be summarized as follows. The investigations of the hadronic observables exhibit that EPOS does not deliver enough hadronic energy to the observation level and the energy per hadron seems to be too small. In the  $N_e - N_\mu$  plane the EPOS showers are shifted to lower electron and higher muon numbers relative to QGSJET 01. When the mass composition of cosmic rays is derived from measured values this effect leads to a relatively light mass composition. In summary, there is a significant discrepancy between the EPOS (version 1.61) predictions and the KASCADE data. The EPOS predictions are not compatible with the measurements.

Most likely the incompatibility of the EPOS predictions with the KASCADE measurements is caused by too high inelastic cross sections for hadronic interactions implemented in the EPOS code. To illustrate this, the proton-air and neutron-carbon cross sections as predicted by different models are displayed in Fig.10. It can be recognized that the EPOS 1.61 values mark the upper limit of the variations exhibited by the different models. Already at moderate energies in the 100 GeV regime a clear difference between the models is visible. In particular, the example of the neutron-carbon cross section illustrates that even at energies accessible to today's accelerator experiments, the models contain different descriptions of the inelastic hadronic cross sections. According to the authors of the EPOS code, a new version is in preparation with lower cross sections. It is expected that the predictions of this version are in better agreement with air shower data. Further studies shall be presented in a follow-up publication.

The results presented also underline the importance of measuring hadronic observables in air shower experiments. They provide the most sensitive available means of investigating the properties of hadronic interactions at very high energies

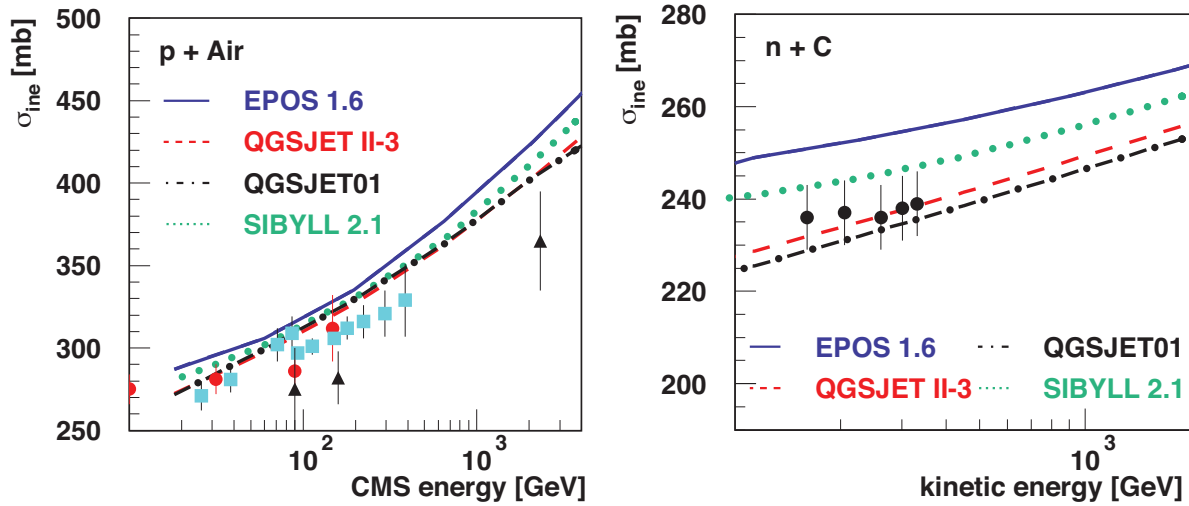


**Figure 10.** Inelastic cross sections for proton-air (*left*) and neutron-carbon (*right*) collisions as predicted by various interaction models. The symbols represent experimental data, left: KASCADE prototype calorimeter (dots) [31], Yodh et al. (squares) [32], ARGO-YBJ (triangles  $\sim 100$  GeV) [33] and EAS-TOP (triangle  $\sim 2000$  GeV) [34]; right: Roberts et al. [35].

and kinematical ranges to complement accelerator experiments.

## Acknowledgement

The authors would like to thank the members of the engineering and technical staff of the KASCADE-Grande collaboration, who contributed to the success of the experiment. The KASCADE-Grande experiment is supported by the BMBF of Germany, the MIUR and INAF of Italy, the Polish Ministry of Science and Higher Education, and the Romanian Ministry of Education and Research (grant CEEEX 05-D11-79/2005).

## References

- [1] T. Antoni et al. *Astropart. Phys.*, 24:1, 2005.
- [2] G. Navarra et al. *Proc. 28th Int. Cosmic Ray Conf., Tsukuba*, 1:147, 2003.
- [3] T. Antoni et al. *Astropart. Phys.*, 16:245, 2002.
- [4] S.P. Swordy et al. *Astropart. Phys.*, 18:129, 2002.
- [5] J.R. Hörandel. *Astropart. Phys.*, 19:193, 2003.
- [6] J.R. Hörandel. *J. Phys. G: Nucl. Part. Phys.*, 29:2439, 2003.
- [7] T. Antoni et al. *J. Phys. G: Nucl. Part. Phys.*, 25:2161, 1999.
- [8] W.D. Apel et al. *J. Phys. G: Nucl. Part. Phys.*, 34:2581, 2007.
- [9] R. Engel. *Nucl. Phys. B (Proc. Suppl.)*, 151:437, 2006.
- [10] D. Heck et al. Report FZKA 6019, Forschungszentrum Karlsruhe, 1998.
- [11] H. Fesefeldt. Report PITHA-85/02, RWTH Aachen, 1985.
- [12] A. Fasso et al. CERN-2005-10, INFN/TC-05/11, SLAC-R-773, 2005.
- [13] A. Fasso et al. arXiv:hep-ph/0306267, 2003.
- [14] J. Ranft. *Phys. Rev. D*, 51:64, 1995.
- [15] N.N. Kalmykov et al. *Nucl. Phys. B (Proc. Suppl.)*, 52B:17, 1997.

- [16] S.S. Ostapchenko. *Phys. Rev. D*, 74:014026, 2006.
- [17] S.S. Ostapchenko. *Nucl. Phys. B (Proc. Suppl.)*, 151:143 and 147, 2006.
- [18] R. Engel et al. *Proc. 26th Int. Cosmic Ray Conf., Salt Lake City*, 1:415, 1999.
- [19] K. Werner, F.M. Liu, and T. Pierog. *Phys. Rev. C*, 74:044902, 2006.
- [20] T. Pierog and K. Werner. arXiv:astro-ph 0611311, 2006.
- [21] T. Antoni et al. *Nucl. Instr. & Meth. A*, 513:490, 2003.
- [22] K. Werner. *Phys. Rep.*, 232:87, 1993.
- [23] J. Engel et al. *Phys. Rev. D*, 46:5013, 1992.
- [24] H.J. Drescher et al. *Phys. Rep.*, 350:93, 2001.
- [25] M. Hladik et al. *Phys. Rev. Lett.*, 86:3506, 2001.
- [26] J. Engler et al. *Nucl. Instr. & Meth. A*, 427:528, 1999.
- [27] S. Plewnia et al. *Nucl. Instr. & Meth. A*, 566:422, 2006.
- [28] T. Antoni et al. *Astropart. Phys.*, 14:245, 2001.
- [29] Geant 3.21 detector description and simulation tool. CERN Program Library Long Writeup W5013, CERN, 1993.
- [30] H. Ulrich et al. *Nucl. Phys. B (Proc. Suppl.)*, 175-176:273, 2008.
- [31] H.H. Mielke et al. *J. Phys. G: Nucl. Part. Phys.*, 20:637, 1994.
- [32] G.B. Yodh et al. *Phys. Rev. D*, 27:1183, 1983.
- [33] I. De Mitri et al. *Proc. 30th Int. Cosmic Ray Conf., Merida*, in press, 2007.
- [34] M. Aglietta et al. *Proc. 30th Int. Cosmic Ray Conf., Merida*, in press, 2007.
- [35] T.J. Roberts et al. *Nucl. Phys. B*, 159:56, 1979.